Tribological assessment of cold sprayed aluminum-quasicrystal composite coatings

Reza Jafari, Minnamari Vippola, Heli Koivuluoto
Tampere University, Faculty of Engineering and Natural Sciences, Materials Science and Environmental Engineering, Tampere, Finland
reza.jafari@tuni.fi

Jan Cizek, Frantisek Lukac
Institute of Plasma Physics of the Czech Academy of Sciences, Prague, Czech Republic

Ladislav Cvrcek, Matej Buril, Jan Walter
Czech Technical University in Prague, Faculty of Mechanical Engineering, Department of Materials Engineering, Prague, Czech Republic

Jarkko Kiilakoski
Saint-Gobain Coating Solutions, Avignon, France

Mari Honkanen, Minnamari Vippola
Tampere University, Tampere Microscopy Center, Tampere, Finland

Abstract

Cold spray (CS) technology has proven an enormous potential in the production of composite coatings, enabling a production of materials with superior qualities such as enhanced tribological behavior. This study aims to investigate the tribological properties of CS Al-based composite coatings reinforced by quasicrystalline (QC) particles. Two different Al alloys were used as the matrix, AA 6061 and AA 2024, and mixed with Al-based QC particles (Al-Cr-Fe-Cu) at different Al/QC ratios. A room-temperature ball-on-disc test was then used to evaluate the wear resistance of the CS composite coatings in air and compared to those of the CS non-reinforced Al alloy coatings as well as cast counterparts (AA 6061-T6). We have demonstrated that CS could be employed to produce dense and thick Al-QC composites. Further, the addition of the QC particles into the structure increased the wear resistance of the matrix resistance up to 8 times.

Keywords

Cold spraying; particle-reinforcement; wear; Al alloys; microstructure.

Introduction

The CS technology offers a fast and reliable coatings production route, with the additional application also for repairs and additive manufacturing of components (Ref 1,2). The high-speed impact of feedstock powder particles accelerated toward the substrate provides the energy required for their deformation. Should the particle kinetic energies be sufficiently high, they deform and bond with each other, whether by mechanical interlocking or by metallurgical bonding, triggering a coating build-up (Ref 3). The whole CS deposition process takes place in the solid state as the temperature of the particles in the gas stream remains considerably below their melting point.

Consequently, the phases in the original feedstock materials are typically preserved in the final coating, in contrast to high temperature thermal spray processes (Ref 3–5). These features highlight CS as a solution for deposition of heat-sensitive materials.

Indeed, cold spraying has been extensively used in deposition of Al and Al alloys (Ref 6). Despite the increasing demand and variety of Al alloy applications, their tribological characteristics might still present a bottleneck (Ref 7). This issue can be solved by incorporating a reinforcing phase into the coating structure. For this, hard phases such as diamond, SiC, WC, or Al_2O_3, have been demonstrated to provide significant mechanical and tribological improvements to cold sprayed metallic Mg, Ti, Ni, Al, or Cu coatings (Ref 4,8–11). The beneficial effect of the hard/heavy particle addition does not stem only from their inherent mechanical or tribological properties, but also includes additional synergistic factors, such as more pronounced deformation of the CS coatings via tamping of the previously deposited materials, leading to a reduction of porosity or grain refinement. As an outcome, e.g., the wear behavior may be improved (Ref 11–13). An alternative route to enhance the tribological properties is through incorporation of low friction materials into the coatings. This approach was observed, e.g., in (Ref 14), where the incorporation of graphene nanoplates into CS Inconel 718 reduced the wear rate and friction coefficient due to the intrinsic lubricity of the graphene. Needless to say, this approach opens the potential of the composite coatings to be used in applications where the tribological properties are essential (Ref 15), such as engine cylinders, discs and pistons.

Ever since the discovery of quasicrystalline materials in 1984 (Ref 16), their potential applications have been widely investigated (Ref 17,18). Notably, the recent QC studies have shown their potential in wear resistant applications (Ref 19,20). As an intermetallic complex compound, high hardness and reduced friction are the features that highlight the QC

tribological properties (Ref 17,21–23). However, their inherent brittleness remains a technical challenge for the industrial applications if used standalone (Ref 20). Therefore, it was suggested to exploit QC as the reinforcing phase in composite structures instead (Ref 24,25). This idea has been implemented in several studies, for instance a successful strengthening of Al matrix nano-composites by Al-Cu-Fe QC reinforcements (Ref 26), CuSn matrix by Al-Cu-Fe-B QC (Ref 27), or superior tribological performance of Ti matrix with Al-Cr-Fe QC particles (Ref 28).

In our previous work (Ref 29), during artificial defect formation on the coating surfaces by abrasive particles, the composite coatings showed a higher resistance against volume loss by erosion compared to non-reinforced CS AA 6061 coatings. Following up on the results, this work aims to investigate and quantify the tribological properties of the CS Al-based composite coatings reinforced by QC particles. Two Al-based alloys, AA 6061 and AA 2024 were mixed with the Al-based QC powders of two different particle sizes. Despite the fact that the QC generally possess a high hardness, thick and dense coatings were successfully deposited using the CS process. The beneficial effect of the QC additional was quantified and the underlying physical phenomena governing the improvement were identified.

Materials and Methods

The QC feedstock material used in this work was an atomized Al-based quasicrystalline powder (Al-Cr-Fe-Cu, Cristome A1, Saint-Gobain Coating Solutions, Avignon, France). More details regarding the chemical composition can be found in (Ref 29). To comprehend the anticipated effect of the QC particle size, two particle size distributions were used: 20–53 µm referred to as the coarser (*cQC)* and 10–30 µm, referred to as the finer (*fQC)*. Gas atomized AA 6061 (10–40 µm) and AA 2024 (15–45 µm) powders from TLS Technik GmbH (Bitterfeld, Germany) were used to formulate the powder blends (Table 1) as well as to deposit the reference coatings. The feedstock blends for composite coatings were prepared by physical mixing of the desired volumetric ratio of the QC powders and AA powders in separate containers.

Grit blasted AA 6082 plates (alumina grit, mesh 24) were used as the substrates and fixed at a constant 40 mm stand-off distance from the cold spray nozzle. High-pressure PCS-100 (Plasma Giken Co., Ltd., Saitama, Japan) cold spray system with N_2 as the propeller gas was used to deposit the coatings, with the deposition parameters optimized in earlier spray trials (Table 1).

The tribological properties were tested using the TRB-S-CE-0000 tribometer (CSM Instruments, Switzerland) in a ball-on-disk arrangement. An Al_2O_3 ball with a diameter of 6 mm was used as a friction counterpart on the mirror polished surface of the coatings. To broaden our understanding of the results, a metallurgical AA 6061-T6 was used in the wear tests as another benchmark. The surfaces of the samples and the Al_2O_3 balls were cleaned with acetone prior to each testing. A normal load of 1 N was used and the linear sliding speed was set to 50 mm/s. The tests were performed at a turning radius of 5 mm with a number of 5000 laps in the air. The friction coefficient, µ, was calculated from the ratio of the tangential friction force and the normal force. After the tests, the surface of the Al_2O_3 balls and the wear tracks were analyzed using a DSX1000 digital microscope (Olympus, Japan). In more detail, the wear track profile was further analyzed using a NewView 7200 optical profilometer (Zygo, USA). Following the method of Archard, the wear rate was calculated as $k = V / F \cdot s$. (Ref 30), where k is the wear rate, V is the wear volume, F is the normal load and s is the sliding distance. The wear volume was obtained by multiplying the area of the wear track cross-section and the circumference of the wear track.

The morphology of the feedstock materials, cross-section of the CS coatings and the wear tracks were analyzed by Zeiss ULTRA plus field emission scanning electron microscope (Zeiss, Germany) equipped with XMaxN energy dispersive spectrometer (EDS, Oxford Instruments, UK). The cross-sections were made by low-speed cutting followed by standard polishing procedures. For cross-sectional observation of the sprayed coatings using backscattered electron detector (BSE) as well as the EDS analysis, an acceleration voltage of 10 kV was applied. To highlight the superficial features of the samples, the secondary electron (SE) imaging was used with the acceleration voltage reduced to 1–3 kV with the working distance close to 5 mm.

The phase composition of the samples was determined by the powder X-ray diffraction (PXRD) method. The measurements were carried out using a D8 Discover vertical powder θ-θ diffractometer (Bruker AXS, Germany) using Cu Kα radiation with Ni Kβ filter. The diffracted beam was detected by the LynxEye 1D detector. Bragg-Brentano geometry was employed with 0.5° fixed divergent slit for the primary beam. The angular range (2θ) was changed from 15 to 120°, with a step size of 0.03° and the total time in each step of 192 s. Phase identification was done using X'Pert HighScore program which accessed the PDF-4+ database of crystalline phases. Quantitative Rietveld refinement was performed in TOPAS V5, aiming at determination of the relative weight content of all identified phases (Ref 31). The quantification of the quasicrystal content in the sprayed coatings was less straightforward and required a calibration procedure for integral intensities calculation. This was realized using XRD measurement of artificially prepared mixtures of the Al alloy and the QC powders.

Table 1. Sample annotation, composition, and respective CS process parameters (p and T are the pressure and preheating temperature of N₂) used for the deposition. All QC content is provided in volumetric %.

Annotation	Feedstock composition	CS process parameters					
		p (bar)	T (°C)	Step size (mm)	Feed (rpm)	CS gun traverse speed (m/min)	Coating layers
A	AA 6061	40	400	1	1.5	20	4
B	AA 2024	40	450	1	3	10	4
A-90cQC*	AA 6061 + 90% cQC	20	450	1.5	3	5	3
A-50cQC*	AA 6061 + 50% cQC	20	450	1.5	3	5	2
A-50fQC**	AA 6061 + 50% fQC	20	450	1.5	3	5	3
B-50cQC*	AA 2024 + 50% cQC	20	450	1.5	3	5	3

*Coarser distribution of QC powders   ** Finer distribution of QC powders

Results and Discussion

Powder characteristics
Figure 1 presents the particle morphology of the used feedstock powders. All four powders exhibited a spherical or semi-spherical particle morphology, with an infrequent presence of irregular particles. Both AA 6061 and AA 2024 powders included relatively small, micron-sized particles along with the larger particles, indicating a broader distribution, as well as a presence of small satellites adhered to the bigger particles, a consequence of the used gas atomization production method. The QC particles exhibited a more corrugated, if slightly porous surface, visible in particular for the coarser particles.

Coating characteristics
The morphology of the coatings is presented in Fig. 2. Comparing the particle shapes in the coatings to their original geometry shown in Fig. 1, the Al particles underwent significant deformation and flattened markedly in the deposition process. The deformation of the QC particles depended on their relative content in the coatings: for lower content, the QC particles tended to retain the original spherical morphology, with only a limited flattening and an infrequent fragmentation. With increasing QC content, the particles obviously underwent an increased level of deformation and an intensified fragmentation, triggering an occurrence of small, standalone fragments in the coatings.

The two non-reinforced coatings, A and B, exhibited relatively higher levels of porosity, predominantly located at the particle boundaries (inset micrographs in Fig. 2). The presence of the QC particles aided in the coating densification by sealing such pores. Importantly, no new pores were formed at the Al matrix-QC boundaries, testifying to the good coherence of the two phases.

Regardless of the Al matrix phase, the QC particles were homogeneously distributed across the entire coatings thickness, validating the applicability of the CS process for a successful composite coating formation. Due to the (anticipated) selective deposition efficiency, the QC particles content in the coatings decreased as compared to the initial feedstock (Table 2).

Increasing the QC content, the following phenomena might have been triggered as discussed in (Ref 10): i) hammering of the underlying structure and pore elimination, ii) incorporation of the fragments from rebounded or cracked particles, and iii) the soft phase interlocking and bonding to the fragments. Ultimately, these could lead to the observed deformation and fragmentation of the QC particles retained in the coatings, as illustrated in the inset image of A-90cQC in Fig. 2, representing a trapped fractured QC powder in the surrounding softer Al phase with highly deformed and refined grains.
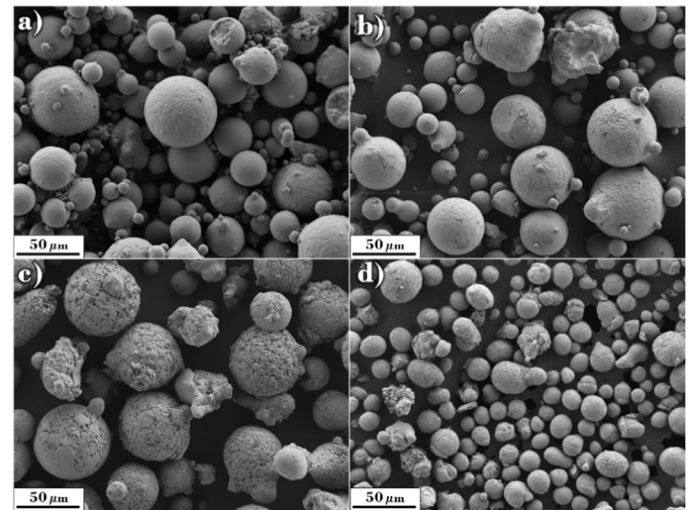

Figure 1. SEM images (SE) showing the morphology of the used powder feedstock particles: a) AA 6061, b) AA 2024, c) coarse QC, d) fine QC.

Both grain refinement and the QC content are potentially interesting features for the tribological properties enhancement.
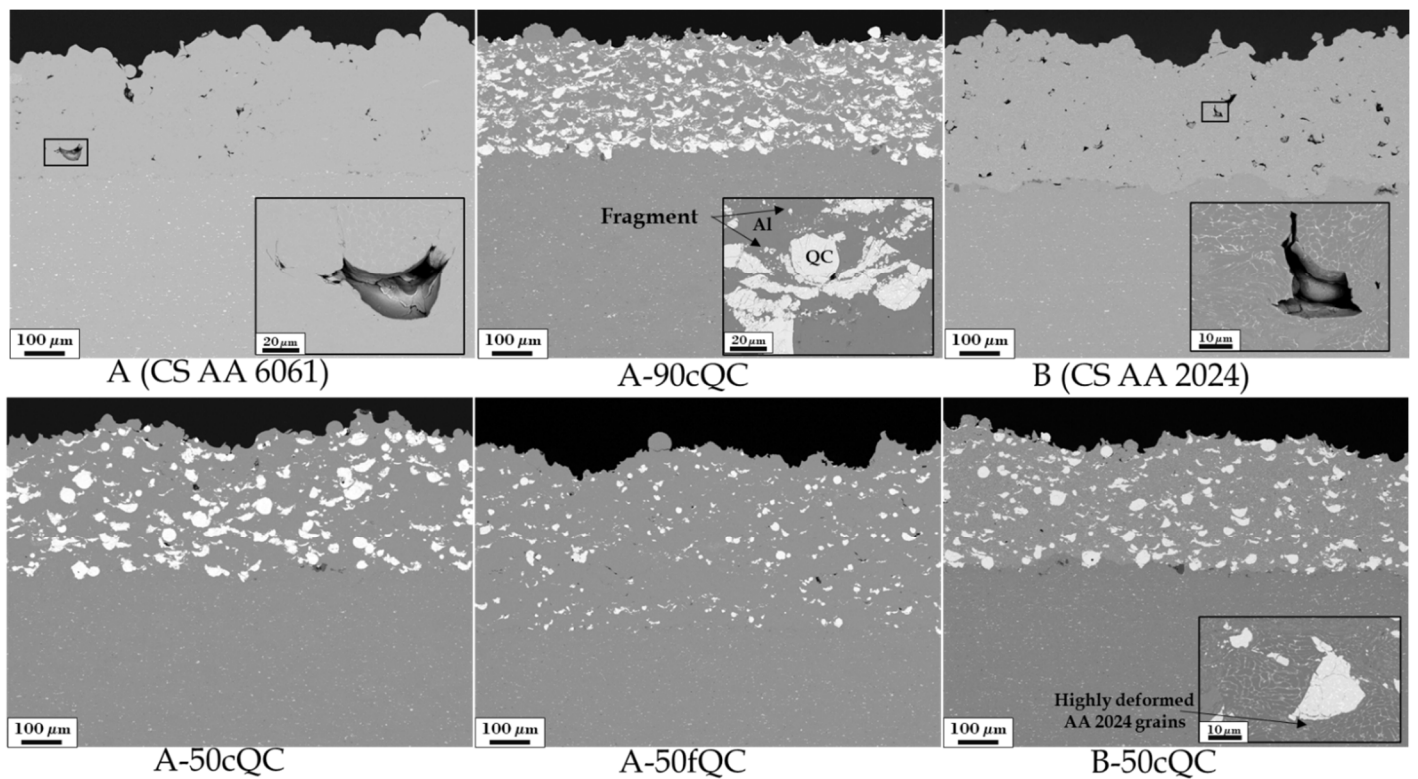
Figure 2. Cross -sectional SEM (BSE) images of the as-sprayed coatings. The provided insets represent magnified views of the area of interest.

Phase constituents

The XRD analysis of the quasicrystalline powder confirmed they mostly comprise of a phase identified as icosahedral isomorphous with the Al13-Cr3-Cu4 (PDF #00-048-1562, (Ref 32)). Since a quasicrystalline phase does not have a translational symmetry and therefore no unit cell available for the Rietveld quantification, the QC phase amounts in the coatings provided in Table 2 were calculated from integral intensities of selected peaks normalized to the reference samples of mixed feedstock powders as described in the *Materials and Methods* section.

From the results, several interesting conclusions can be drawn. First, the effectiveness of retaining the fine QC content in the coating structure was significantly lower when compared to retention of the coarse QC phase (cf. A-50fQC and A-50cQC). This could potentially be attributed to the fact that the same number of retained larger particles yields a higher QC content when compared with the cumulative retained volume of the same number of fine particles. Second, comparing the A-50cQC and B-50cQC coatings, it seems that the AA 6061 alloy matrix is more efficient in retaining the quasicrystals in the composite. The possible reason might be the lower hardness of the CS AA 6061 as compared to that of CS AA 2024, enabling a higher deformation capacity for the QC particles incorporation. Third, increasing the QC content in the feedstock from 50 vol.% to 90 vol.% (i.e., an +80% increase) led to an increase of approximately +55% in the coatings. This is connected to the selective deposition efficiency; with a higher QC content, the probability of non-effective impacts (i.e., QC particles rebounded on QC particles) increases.

Wear performance

The friction coefficient and the wear rate of the samples were calculated by sliding of a 6 mm diameter Al_2O_3 ball counterpart over the polished sample surfaces. After the running-in phase, the average μ was in the range of 0.5–0.6 for all tested samples (Fig. 4). The friction coefficient for the cast and cold-sprayed AA 6061 was almost the same. However, compared to the other samples, these two samples exhibited a much longer running-in phase that ultimately stabilized to lower values. A similar behavior was observed in testing of CS Al-nano-diamond composites (Ref 33). It is interesting to note that in that study, the coefficient of friction started from the lower values and increased during run-in phase after the heat-treatment.

Figure 5 clearly indicates the effect of QC addition on the wear rate and wear track width of the tested coatings. The wear performance was evaluated from the wear track width first, where the beneficial effect of quasicrystals was confirmed. Both Al-alloy matrices always had a larger wearing, manifested by the greater wear track widths than the QC-reinforced composites. For these, there was no wrapping of the aluminum component on the ball, the run-in phase is shortened, and the resulting wear rates were several times lower.

Of the composite coatings, the A-50fQC had the highest wear rate and track width. One of the reasons could be the lowest actual QC content among the coatings, amounting to 11 wt.% only. As the amount of QC in the composite structure increased, the wear rate was expected to decrease. However, the recorded decrease was relatively small, not fully corresponding to the QC content increase.
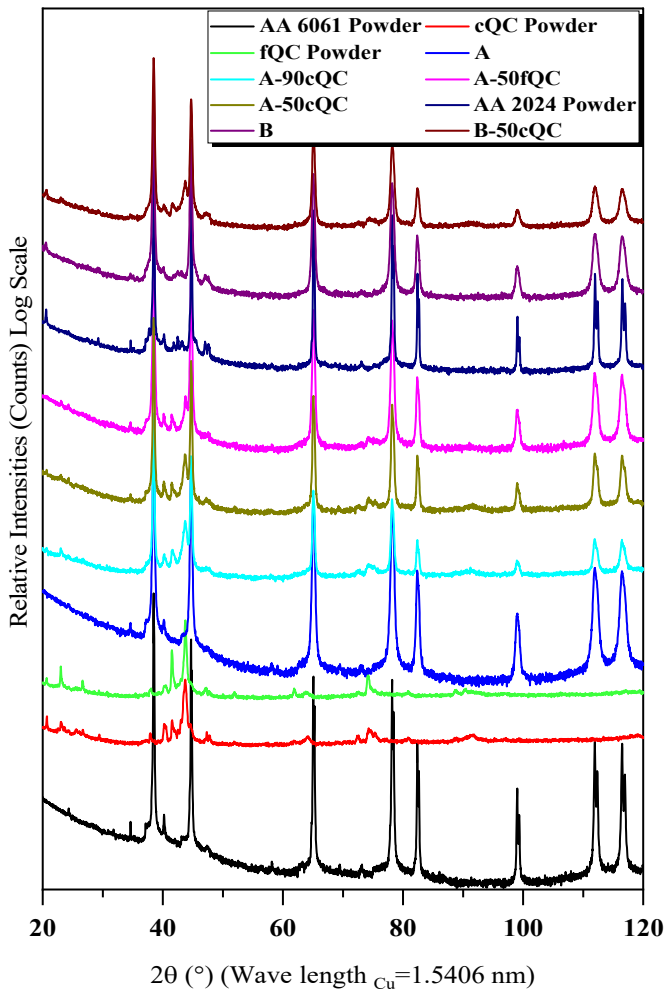
Figure 3. XRD spectra of the powder feedstocks and the cold sprayed coatings.

Figure 4. The friction coefficients of the samples tested against the Al_2O_3 ball.

Figure 5. The wear rates (green bars) and the wear tracks widths (blue scatter symbols) of the tested materials.

Table 2. Composition of the feedstock powders (given in volumetric percent) and the coatings (given in weight percent as determined by XRD).

Sample	QC in feedstock (vol.%)	QC in coating (wt.%)
A-50cQC	50	31
B-50cQC	50	24
A-90cQC	90	48
A-50fQC	50	11

Importantly, all composite structures showed wear rates lower than the precipitation-hardened bulk AA 6061-T6. As compared to the cold sprayed matrix, the improvement of the A-90cQC sample was +792%, a rather significant enhancement of the tribological properties. The improvement was as high as +707 % for A-50cQC, +420 % for A-50fQC, and +368 % for B-50cQC. The enhancement percentages are calculated as the ratio of the wear rates of A and B to the wear rates of the corresponding reinforced composite coatings. Comparison of these values clearly indicated that the softer AA 6061 benefited more from the QC incorporation in the structure by CS.
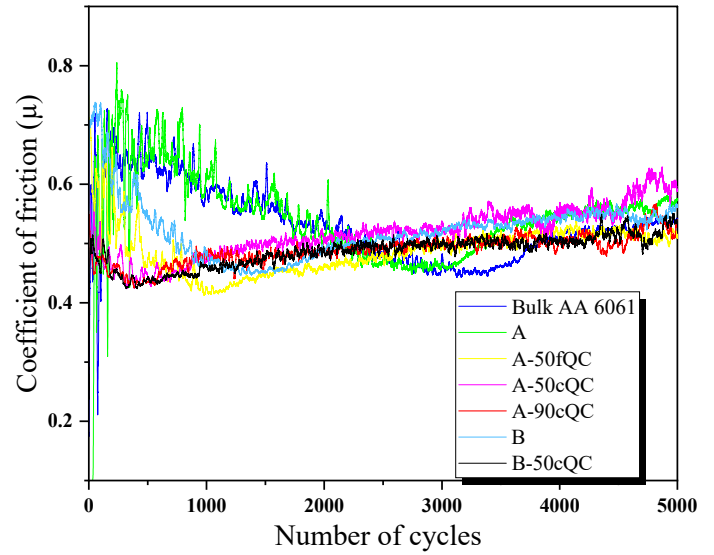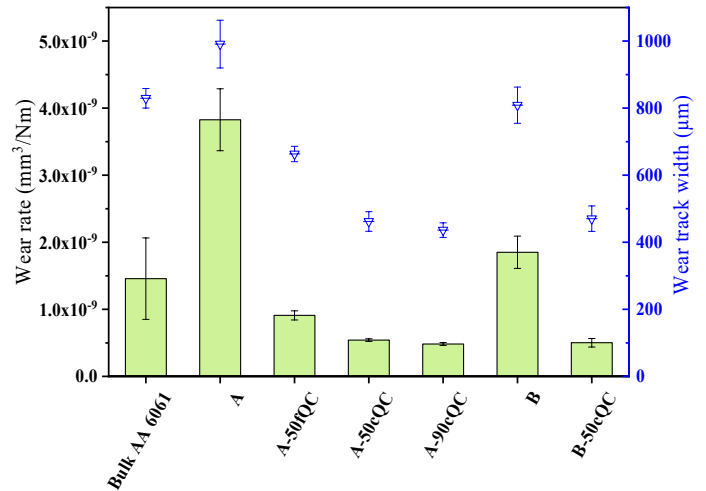
The best and worst performing coating samples, A-90cQC and A (CS AA 6061), were selected for a subsequent residual wear tracks characterization and compared to that of the bulk AA 6061-T6 sample. Fig. 6 provides the corresponding micrographs and EDS analysis of the features observed on the studied wear track surfaces. The A-90cQC sample with the highest wear resistance had a significantly narrower wear region. The combination of several factors such as high content of the harder QC particles, and the tamping-induced grain refinement and pore elimination triggered the remarkable decline of wear damage compared to both Al alloy counterparts (Ref 11–13). The higher magnification micrographs presented in Fig. 6 contain evidence of a ductile deformation of the AA 6061 matrix as the governing factor in the wear mechanism. The agglomerated debris found locally inside the groove were generally oxidized metallic elements as confirmed by the EDS results. Nevertheless, most of the wear tracks were composed of a smooth tribofilm with a localized spallation.
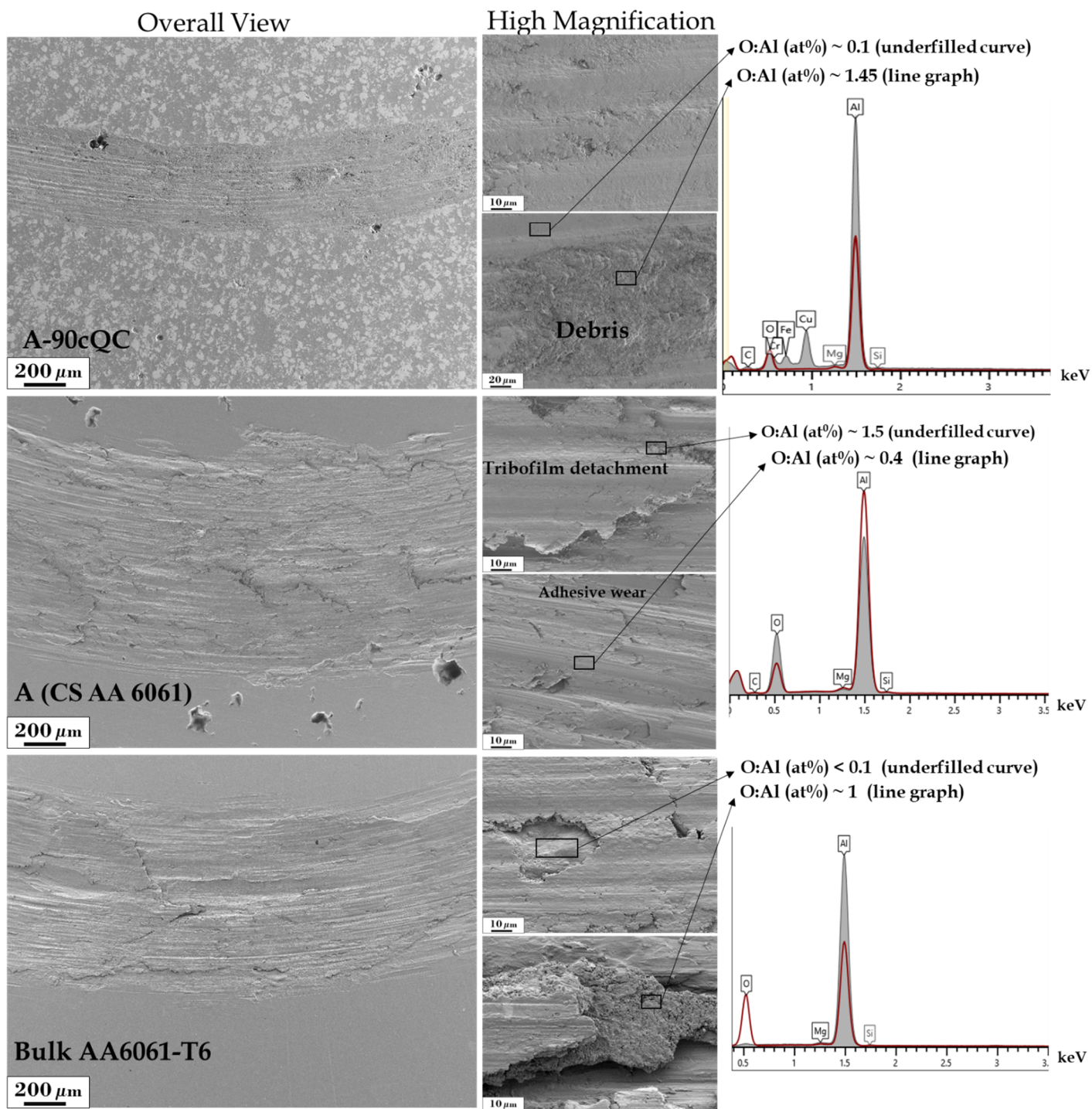
Figure 6. A detailed wear track characterization of the best and worst wear-performing CS samples compared to the bulk metallurgical counterpart using SEM (SE) images and EDS. The atomic% ratio of O to Al for each EDS graph is reported as a measure of oxidation.

Interestingly, no visible signs of the reinforcing particle pull-outs were found in the observed regions, indicating a good coherence between the Al matrix and the QC particles. The EDS analysis from the smoother region showed Cu, Cr and Fe signals, i.e., elements originally present in the QC particles. This would indicate either a surface exposure or sub-surface presence of QC particles. A possible explanation for the lower friction coefficient in the running-in period can be the low friction nature of the QC particles that are in contact with the Al_2O_3 ball before formation of the tribofilm and reaching the steady state. In contrast, the residual wear groove of the CS AA 6061 with the lowest wear resistance mainly consisted of a spalled, Al-rich oxide tribofilm. As observed by SEM and also the optical profilometer, the CS Al 6061 coating and Al 6061 bulk exhibited formation of parallel grooves along the wear direction deeper than similar grooves formed on the composite samples. Here, the tribofilm consists of Al-rich oxides with local spallation and detachment, exposing the non-oxidized metal surface. The cycle of tribofilm formation and subsequent

film detachment under the load of the counterface could be responsible for the significance of the wear loss (Ref 34).

To sum up, both CS and bulk AA 6061 showed a similar wear track morphology with a smeared appearance identified as adhesive wear (Ref 33). Even though the adhesive wear was not observed on the surface of the Al_2O_3 ball counterpart, the morphology was similar to previous investigation on Al wear performance (Ref 33). The difference in wear behavior between the CS coatings and bulk materials could be potentially attributed to the presence of interparticle boundaries that might weaken the cohesion between the Al particles in CS coating under sliding load and higher density of the bulk, precipitation-hardened AA 6061-T6. On the other hand, less smearing in the wear track and a presence of oxidized metallic debris in the case of the A-90cQC composite surface would suggest an activation of the abrasive wear mechanism (Ref 33). The reduction of adhesive wear and a transition to the abrasive wear resulted in a lower wearing of the composite coatings (Ref 34). Despite earlier results suggesting a low friction QC materials (Ref 20,28), no remarkable reduction of the friction coefficient was observed in the current study. However, the run-in phase for QC-containing composite structure were accompanied with a lower friction coefficient, μ, compared to the final state. It can be speculated that in the earlier stages when there was a direct contact between the Al_2O_3 counterface and the QC phases, the low friction nature of the QC was the governing factor. In the later cycles when the oxidized surface encountered the Al_2O_3 ball, the μ value was stabilized in a close range for the tested materials.

Conclusions and future works

Cold sprayed composite coatings made of Al alloys reinforced by Al-based QC phases exhibited remarkable enhancement of wear resistance. The wear rate and wear track width values were significantly decreased by incorporation of QC particles in the initial blend of the powder feedstock materials and consequently in the coatings. The best performing coating exhibited a remarkable +792 % improvement of wear rate as opposed to the non-reinforced Al alloy. In this study, QC incorporation was more beneficial with AA 6061 matrix compared to the AA 2024 matrix, having higher wear resistance improvements. In addition, larger QC particles were more effective in improving wear resistance. The microstructural studies along with wear performance assessments indicated that QC incorporation triggered the transition from adhesive wear to abrasive wear mechanisms.

Acknowledgments

References

1. X. Xie, S. Yin, R. nirina Raoelison, C. Chen, C. Verdy, W. Li, G. Ji, Z. Ren, and H. Liao, Al Matrix Composites Fabricated by Solid-State Cold Spray Deposition: A Critical Review, *J. Mater. Sci. Technol.*, Elsevier Ltd, 2021, **86**, p 20–55, doi:10.1016/j.jmst.2021.01.026.
2. S. Yin, P. Cavaliere, B. Aldwell, R. Jenkins, H. Liao, W. Li, and R. Lupoi, Cold Spray Additive Manufacturing and Repair: Fundamentals and Applications, *Addit. Manuf.*, Elsevier, 2018, **21**(August 2017), p 628–650, doi:10.1016/j.addma.2018.04.017.
3. T. Schmidt, F. Gärtner, H. Assadi, and H. Kreye, Development of a Generalized Parameter Window for Cold Spray Deposition, *Acta Mater.*, 2006, **54**(3), p 729–742.
4. H. Koivuluoto, G. Bolelli, A. Milanti, L. Lusvarghi, and P. Vuoristo, Microstructural Analysis of High-Pressure Cold-Sprayed Ni, NiCu and NiCu + Al2O3 Coatings, *Surf. Coatings Technol.*, Elsevier B.V., 2015, **268**, p 224–229, doi:10.1016/j.surfcoat.2014.09.007.
5. S. Yin, J. Cizek, J. Cupera, M. Hassani, X. Luo, R. Jenkins, Y. Xie, W. Li, and R. Lupoi, Formation Conditions of Vortex-like Intermixing Interfaces in Cold Spray, *Mater. Des.*, The Authors, 2021, **200**, p 109444, doi:10.1016/j.matdes.2020.109444.
6. D. Guo, M. Kazasidis, A. Hawkins, N. Fan, Z. Leclerc, D. MacDonald, A. Nastic, R. Nikbakht, R. Ortiz-Fernandez, S. Rahmati, M. Razavipour, P. Richer, S. Yin, R. Lupoi, and B. Jodoin, Cold Spray: Over 30 Years of Development Toward a Hot Future, *J. Therm. Spray Technol.*, Springer US, 2022, doi:10.1007/s11666-022-01366-4.
7. D. Cruz, M.Á. Garrido, Á. Rico, C.J. Múnez, and P. Poza, Wear Resistance of Cold Sprayed Al Alloys for Aeronautical Repairs, *Surf. Eng.*, Taylor & Francis, 2019, **35**(4), p 295–303, doi:10.1080/02670844.2018.1427318.
8. R. Fernandez and B. Jodoin, Cold Spray Aluminum–Alumina Cermet Coatings: Effect of Alumina Morphology, *J. Therm. Spray Technol.*, Springer US, 2019, **28**(4), p 737–755, doi:10.1007/s11666-019-00845-5.
9. Q. Wang, K. Spencer, N. Birbilis, and M. Zhang, Surface & Coatings Technology The in Fl Uence of Ceramic Particles on Bond Strength of Cold Spray Composite Coatings on AZ91 Alloy Substrate, *Surf. Coat. Technol.*, Elsevier B.V., 2010, **205**(1), p 50–56, doi:10.1016/j.surfcoat.2010.06.008.
10. A.W.Y. Tan, J.Y. Lek, W. Sun, A. Bhowmik, I. Marinescu, P.J. Buenconsejo, Z. Dong, and E. Liu, Microstructure, Mechanical and Tribological Properties of Cold Sprayed Ti6Al4V–CoCr Composite Coatings, *Compos. Part B Eng.*, Elsevier Ltd, 2020, **202**(July), p 108280, doi:10.1016/j.compositesb.2020.108280.
11. S.A. Alidokht and R.R. Chromik, Sliding Wear Behavior of Cold-Sprayed Ni-WC Composite Coatings: Influence OF WC Content, *Wear*, Elsevier B.V., 2021, **477**(November 2020), p 203792, doi:10.1016/j.wear.2021.203792.
12. R. Nikbakht, M. Saadati, T.-S. Kim, M. Jahazi, H.S. Kim, and B. Jodoin, Cold Spray Deposition Characteristic and Bonding of CrMnCoFeNi High Entropy Alloy, *Surf. Coatings Technol.*, Elsevier B.V., 2021, **425**(October), p 127748, doi:10.1016/j.surfcoat.2021.127748.
13. S. Yin, J. Cizek, C. Chen, R. Jenkins, G. O'Donnell, and R. Lupoi, Metallurgical Bonding between Metal Matrix and Core-Shelled Reinforcements in Cold Sprayed Composite Coating, *Scr. Mater.*, Elsevier Ltd, 2020, **177**, p 49–53, doi:10.1016/j.scriptamat.2019.09.023.
14. W. Sun, A.W.-Y. Tan, A. Bhowmik, F. Xue, I. Marinescu, and E. Liu, Evaluation of Cold Sprayed Graphene

Nanoplates–Inconel 718 Composite Coatings, *Surf. Coatings Technol.*, 2019, **378**, p 125065, doi:10.1016/j.surfcoat.2019.125065.

15. P. Poza and M.Á. Garrido-Maneiro, Cold-Sprayed Coatings: Microstructure, Mechanical Properties, and Wear Behaviour, *Prog. Mater. Sci.*, 2022, **123**(June 2020).

16. D. Shechtman, I. Blech, D. Gratias, and J.W. Cahn, Metallic Phase with Long-Range Orientational Order and No Translational Symmetry, *Phys. Rev. Lett.*, 1984, **53**(20), p 1951–1953, doi:10.1103/PhysRevLett.53.1951.

17. E. Huttunen-Saarivirta, Microstructure, Fabrication and Properties of Quasicrystalline Al-Cu-Fe Alloys: A Review, *J. Alloys Compd.*, 2004, **363**(1–2), p 154–178.

18. J.M. Dubois, So Useful, Those Quasicrystals, *Isr. J. Chem.*, 2011, **51**(11–12), p 1168–1175.

19. B.A. Silva Guedes de Lima, R. Medeiros Gomes, S.J. Guedes de Lima, D. Dragoe, M.G. Barthes-Labrousse, R. Kouitat-Njiwa, and J.M. Dubois, Self-Lubricating, Low-Friction, Wear-Resistant Al-Based Quasicrystalline Coatings, *Sci. Technol. Adv. Mater.*, Taylor & Francis, 2016, **17**(1), p 71–79, doi:10.1080/14686996.2016.1152563.

20. W. Wolf, G.Y. Koga, R. Schulz, S. Savoie, C.S. Kiminami, C. Bolfarini, and W.J. Botta, Wear and Corrosion Performance of Al-Cu-Fe-(Cr) Quasicrystalline Coatings Produced by HVOF, *J. Therm. Spray Technol.*, Springer US, 2020, **29**(5), p 1195–1207, doi:10.1007/s11666-020-01053-2.

21. T.P. Yadav and N.K. Mukhopadhyay, Quasicrystal: A Low-Frictional Novel Material, *Curr. Opin. Chem. Eng.*, Elsevier Ltd, 2018, **19**, p 163–169, doi:10.1016/j.coche.2018.03.005.

22. K. Lee, J. Hsu, D. Naugle, and H. Liang, Multi-Phase Quasicrystalline Alloys for Superior Wear Resistance, *Mater. Des.*, Elsevier Ltd, 2016, **108**, p 440–447, doi:10.1016/j.matdes.2016.06.113.

23. D.A. Rabson, Toward Theories of Friction and Adhesion on Quasicrystals, *Prog. Surf. Sci.*, Elsevier Ltd, 2012, **87**(9–12), p 253–271, doi:10.1016/j.progsurf.2012.10.001.

24. W. Wolf, F.G. Coury, M.J. Kaufman, C. Bolfarini, C.S. Kiminami, and W.J. Botta, The Formation of Quasicrystals in Al-Cu-Fe-(M=Cr,Ni) Melt-Spun Ribbons, *J. Alloys Compd.*, Elsevier B.V, 2018, **731**, p 1288–1294, doi:10.1016/j.jallcom.2017.09.139.

25. W. Wolf, C. Bolfarini, C.S. Kiminami, and W.J. Botta, Recent Developments on Fabrication of Al-matrix Composites Reinforced with Quasicrystals: From Metastable to Conventional Processing, *J. Mater. Res.*, Springer International Publishing, 2021, **36**(1), p 281–297, doi:10.1557/s43578-020-00083-4.

26. Y. Shadangi, S. Sharma, V. Shivam, J. Basu, K. Chattopadhyay, B. Majumdar, and N.K. Mukhopadhyay, Fabrication of Al–Cu–Fe Quasicrystal Reinforced 6082 Aluminium Matrix Nanocomposites through Mechanical Milling and Spark Plasma Sintering, *J. Alloys Compd.*, Elsevier B.V, 2020, **828**, p 154258, doi:10.1016/j.jallcom.2020.154258.

27. X. Guo, J. Chen, H. Yu, H. Liao, and C. Coddet, A Study on the Microstructure and Tribological Behavior of Cold-Sprayed Metal Matrix Composites Reinforced by Particulate Quasicrystal, *Surf. Coatings Technol.*, Elsevier B.V., 2015, **268**, p 94–98, doi:10.1016/j.surfcoat.2014.05.062.

28. N.W. Khun, R.T. Li, K. Loke, and K.A. Khor, Effects of Al-Cr-Fe Quasicrystal Content on Tribological Properties of Cold-Sprayed Titanium Composite Coatings, *Tribol. Trans.*, 2015, **58**(4), p 616–624.

29. R. Jafari, J. Kiilakoski, M. Honkanen, M. Vippola, and H. Koivuluoto, Wetting Behavior and Functionality Restoration of Cold-Sprayed Aluminum-Quasicrystalline Composite Coatings, *J. Therm. Spray Technol.*, 2023, doi:10.1007/s11666-022-01522-w.

30. J.F. Archard, Contact and Rubbing of Flat Surfaces, *J. Appl. Phys.*, 1953, **24**(8), p 981–988.

31. H.M. Rietveld, Line Profiles of Neutron Powder-Diffraction Peaks for Structure Refinement, *Acta Crystallogr.*, 1967, **22**(1), p 151–152, doi:10.1107/S0365110X67000234.

32. A.-P. Tsai, A. Inoue, and T. Masumoto, New Quasicrystals in Al65Cu20M15 (M = Cr, Mn or Fe) Systems Prepared by Rapid Solidification, *J. Mater. Sci. Lett.*, 1988, **7**(4), p 322–326, doi:10.1007/BF01730730.

33. A. Loganathan, S. Rengifo, A.F. Hernandez, C. Zhang, and A. Agarwal, Effect of Nanodiamond Reinforcement and Heat-Treatment on Microstructure, Mechanical and Tribological Properties of Cold Sprayed Aluminum Coating, *Surf. Coatings Technol.*, Elsevier B.V., 2021, **412**(December 2020), p 127037, doi:10.1016/j.surfcoat.2021.127037.

34. R.R. Chromik, S.A. Alidokht, J.M. Shockley, and Y. Zhang, Tribological Coatings Prepared by Cold Spray, *Cold-Spray Coatings: Recent Trends and Future perspectives*, 2017, p 321–348.